Sensors and Materials, Vol. 35, No. 2 (2023) 475–481
MYU Tokyo

S & M 3184

Analysis of Photoluminescence and Dosimetric Properties of (Ce, Tb)-codoped Magnesium Orthosilicate Single Crystals

Kensei Ichiba,[1*] Yuma Takebuchi,[1] Hiromi Kimura,[2] Takumi Kato,[1]
Daisuke Nakauchi,[1] Noriaki Kawaguchi,[1] and Takayuki Yanagida[1]

[1]Division of Materials Science, Nara Institute of Science and Technology (NAIST),
8916-5 Takayama, Ikoma, Nara 630-0192, Japan
[2]National Institute of Advanced Industrial Science and Technology (AIST),
1-1-1 Tsukuba, Ibaraki 305-8569, Japan

(Received September 27, 2022; accepted January 12, 2023)

Keywords: storage phosphor, radiation detection, single crystal

In this study, $Mg_{1.995-x}SiO_4$:xCe, 0.005Tb (x = 0 and 0.01) single crystals were synthesized by the floating zone method and their photoluminescence (PL) and dosimetric properties were evaluated. In the PL process, emission peaks due to the 4f–4f transitions of Tb^{3+} ions were observed in the x = 0 and 0.01 samples, and the emission peak due to the 5d–4f transitions of Ce^{3+} ions was detected in the x = 0.01 sample. In the thermally stimulated luminescence (TSL) process, only emission peaks due to the 4f–4f transitions of Tb^{3+} ions were observed in both samples, and the x = 0.01 sample had higher TSL intensity than the x = 0 sample. The x = 0.01 sample showed a lower detection limit of 0.01 mGy and a spatial resolution of 50.0 μm under X-ray irradiation.

1. Introduction

Storage phosphors for ionizing radiation detectors are actively used in a broad range of fields such as medicine,[1] environmental dosimetry,[2] and personal dose monitoring.[3] The storage phosphors can accumulate incident radiation energy. When storage phosphors interact with ionizing radiation, numerous carriers are generated in them. The generated carriers are captured at localized trapping centers. Then, the trapped carriers are released by external stimulation, such as light or heat, and migrate to the luminescence centers. The luminescence caused by light and heat is called optically stimulated luminescence (OSL) and thermally stimulated luminescence (TSL), respectively.[4] The properties required for storage phosphors are high luminescence intensity, low fading, a linear relationship between the radiation dose and the luminescence intensity, and an effective atomic number (Z_{eff}) close to that of human soft tissues (Z_{eff} = 7.29).[5] Currently there are no ideal storage phosphors that have all the above features; therefore, many researchers have continued to develop storage phosphors to improve their properties.[6–12]

*Corresponding author: e-mail: ichiba.kensei.if7@ms.naist.jp
https://doi.org/10.18494/SAM4143

ISSN 0914-4935
https://myukk.org/

Magnesium orthosilicate (Mg_2SiO_4) is a well-known host material of inorganic phosphors because of its stable crystal structure, high physical and chemical stability, and low thermal expansion property.[13] Mg_2SiO_4 is also a well-known material for storing phosphors for personal dosimetry because Z_{eff} of Mg_2SiO_4 (11.4) is relatively close to that of human soft tissues.[14] In particular, Tb-doped Mg_2SiO_4 powders are used as commercial TSL dosimeters. For this reason, many researchers have investigated the TSL properties of Mg_2SiO_4 doped with Tb^{3+} ions.[15–17]

The main aim of this study is to improve the TSL intensity of Tb-doped Mg_2SiO_4. The TSL intensity is generally affected by several factors such as the trapping probability of carriers and the quantum yields (*QY*s) of the luminescence centers.[18] In previous studies, the TSL intensity of Mg_2SiO_4 was improved by codoping with two different rare earths.[19,20] However, Mg_2SiO_4 codoped with Ce^{3+} and Tb^{3+} ions has not been researched, although the utility of this combination has been verified for other host materials.[21–23] Since Ce can take a tetravalent state in addition to a trivalent state, Ce^{3+} and Ce^{4+} ions are expected to act as hole and electron trap centers, respectively, which would improve the TSL intensity.

Furthermore, we also focused on bulk single crystals as the material form. Since single crystals generally have higher transmittance than powders and ceramics, TSL can be obtained from both the surface and inside of the material. In other words, more photons can be detected due to the higher transmittance of the material, which would improve the luminescence intensity.[18,24] For the above reasons, we synthesized Mg_2SiO_4:Ce, Tb single crystals and evaluated their photoluminescence (PL) and dosimetric properties.

2. Materials and Methods

$Mg_{1.995}SiO_4$:0.005Tb ($x = 0$) and $Mg_{1.985}SiO_4$:0.01Ce, 0.005Tb ($x = 0.01$) were grown by the floating zone (FZ) method. The starting powders were MgO (99.99%, High Purity Chemicals), SiO_2 (99.99%, Rare Metallic), CeO_2 (99.99%, Furuuchi Chemical), and Tb_4O_7 (99.99%, Furuuchi Chemical). After these powders were uniformly mixed with an agate mortar and pestle, each mixture was placed in a balloon and compressed into a cylindrical rod using isostatic pressure. Then, each cylindrical rod was sintered at 1400 °C for 8 h using an electric furnace in air to obtain a ceramic rod. Each ceramic rod was set in an FZ furnace (Crystal Systems Corporation, FZ-T-12000-X-VPO-PC-YH) equipped with four xenon arc lamps to grow crystals of $x = 0$ and 0.01 samples. The pull-down rate was 10 mm/h, and the rotation rate was 3 rpm during the crystal growth. Each synthesized crystalline rod was crushed before the measurement of the sample. To identify the crystal phase, the powder X-ray diffraction (PXRD) was examined by a diffractometer (Rigaku, MiniFlex600) in the range of $2\theta = 10–90°$.

The PL excitation/emission maps and *QY*s were evaluated by using a Quantaurus-QY system (Hamamatsu, C11347-01). Considering the results of the PL excitation/mission maps, the PL decay time profiles were measured by another Quantaurus-τ system (Hamamatsu, C11367).

To evaluate the dosimetric properties, TSL glow curves after X-ray irradiation were obtained by using a TSL reader (NanoGray Inc., TL-2000).[25] In the measurements, the temperature

range was 100–490 °C and the heating rate was 1 °C/s. The samples were irradiated by X-rays emitted from an X-ray generator (Spellman, XRB80P&N200X4550). TSL spectra were measured by a CCD-based spectrometer (Ocean Optics, QE Pro) while the samples were heated by an electric heater (Sakaguchi, Ultramic 200 W) and a temperature controller (Sakaguchi, SCR-SHQ-A). The heating rate and temperature range were 1 °C/s and 50–400 °C, respectively. In addition, the TSL dose response functions were evaluated using several TSL glow curves after different irradiated doses from 0.01 to 100 mGy. The TSL dose response functions were obtained from the integration of TSL intensities for each irradiation dose over the temperature range from 100 to 490 °C to account for the influence of fading.

An X-ray imaging test was carried out using our original setup. Each sample was irradiated with X-rays through a Pb-based square test chart (DIAGNOMATIC, Pro-Res RF BarType7). The irradiation dose was 10 Gy from the above-mentioned X-ray generator. Then, the sample was heated to 500 °C by a ceramic hot plate (As One, CHO-170AF), and the emission was read by a CCD camera (BK-54DUV, Bitran Corp.).

3. Results and Discussion

Figure 1(a) shows a photograph of the $x = 0$ and 0.01 samples. Both samples were approximately 4 × 4 × 1 mm^3 and their weights were 64.8 and 40.0 mg, respectively. Both samples were colorless and transparent, although they contained some cracks.

Figure 1(b) shows the PXRD patterns of the $x = 0$ and 0.01 samples. The peak positions of the synthesized samples corresponded to those of the reference data (COD 900319) of Mg_2SiO_4. Therefore, both samples had a single-phase orthorhombic structure. In addition, no peak shifts due to Ce and Tb doping were confirmed, although it has been reported that Mg^{2+} sites in Mg_2SiO_4 can be occupied by Ce and Tb.[26,27] The reason for the absence of peak shifts was the low concentrations of Ce and Tb, which were below the detection threshold of our apparatus.

Figure 2 shows the PL emission/excitation maps of the (a) $x = 0$ and (b) $x = 0.01$ samples. In the $x = 0$ sample, some emission peaks were observed under excitation at 250 nm. Moreover, emission peaks at around 550 nm were also detected under excitation at 370 nm. These emissions originated from the 4f–4f transitions of Tb^{3+} ions.[28] On the other hand, in the $x = 0.01$ sample, emission peaks due to 4f–4f transitions of Tb^{3+} ions

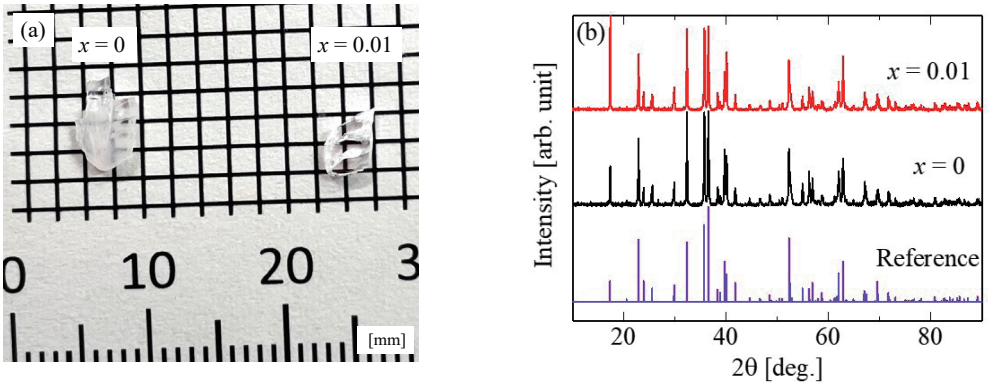

Fig. 1. (Color online) (a) Photograph and (b) PXRD patterns of the synthesized $x = 0$ and 0.01 samples. The reference spectrum was COD 900319.

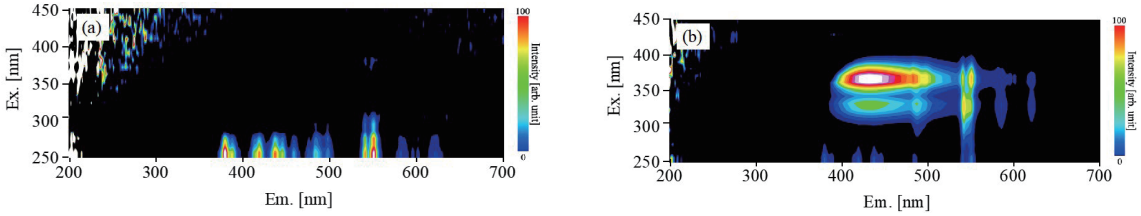

Fig. 2. (Color online) PL emission/excitation maps of the (a) $x = 0$ and (b) $x = 0.01$ samples. The vertical and horizontal axes show excitation and emission wavelengths, respectively.

were observed under excitation at wavelengths of 250, 340, and 370 nm. Furthermore, a broad emission band was observed from 370 to 540 nm under excitation at 340 and 370 nm. This was due to the 5d–4f transitions of Ce^{3+} ions.[29,30] No emission band due to Ce^{3+} ions was observed under excitation at 250 nm. Therefore, no energy transfer from Tb to Ce occurred. The *QY* values of the $x = 0$ and 0.01 samples were 27.0% (Ex. 250 nm) and 40.2% (Ex. 370 nm), respectively.

Figure 3 shows the PL decay time profiles of the $x = 0$ and 0.01 samples monitored at (a) 420 nm under 365 nm excitation and (b) 550 nm under 370 nm excitation. All the decay curves were reproduced by an exponential decay equation. The obtained decay time constant (Ex. 365 nm/Em. 420 nm) of the $x = 0.01$ sample was 45.8 ns, which corresponded to a typical value derived from the 5d–4f transitions of Ce^{3+} ions.[31–33] On the other hand, the decay time constants (Ex. 370 nm/Em. 550 nm) of the $x = 0$ and 0.01 samples were 2.1 and 2.2 ms, respectively, which are typical values for the 4f–4f transitions of Tb^{3+} ions.[34,35]

Figure 4(a) shows the TSL glow curves of the $x = 0$ and 0.01 samples after X-ray irradiation. The intensities of the TSL glow curves were corrected for the weight of each sample. The irradiation dose was 100 mGy. For the $x = 0$ sample, the glow peaks were confirmed at around 190 and 380 °C. The $x = 0.01$ sample had glow peaks at the same temperature as the $x = 0$ sample. Glow peaks at 190 and 380 °C have been reported[29,36,37] and are related to F^+ and F centers, respectively.[38,39] Figure 4(b) shows the TSL spectra of the $x = 0$ and 0.01 samples heated at 190 °C. Both samples had peaks at 380, 420, 440, 460, 480, 495, 550, 590, and 630 nm, which are typical wavelengths due to the 4f–4f transitions of Tb^{3+} ions.[28] In contrast, no peaks due to the 5d–4f transitions of Ce^{3+} ions were detected, whereas the PL properties suggested the existence of Ce^{3+} ions. Thus, it is considered that Ce^{3+} ions did not directly contribute to the TSL process as luminescence centers. The increase in the TSL intensity at 190 and 380 °C is considered to have been caused by the increasing number of F^+ and F centers due to charge compensation between Ce^{3+} and Mg^{2+} ions.

Figure 5(a) illustrates the TSL dose response functions of the $x = 0$ and 0.01 samples. To evaluate their performance as dosimeters, we also plotted the TSL dose response function of a commercial TSL dosimeter (TORECK, MSO-S) equipped with powder-form Tb-doped Mg_2SiO_4. The weight of the powder inserted in MSO-S was 30.1 mg. The vertical axis shows integrated values of the TSL glow curve in the range of 100–490 °C. All the TSL dose response functions were found to have a linear relationship in the range

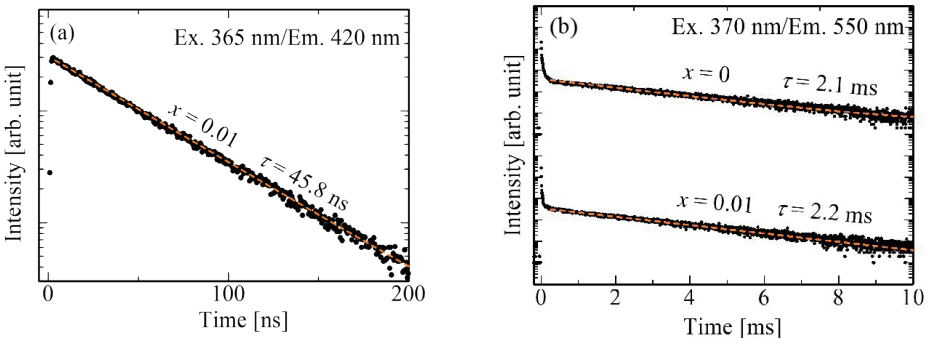

Fig. 3. (Color online) PL decay time profiles of the $x = 0$ and 0.01 samples monitored at (a) 420 nm under 365 nm excitation and (b) 550 nm under 370 nm excitation. Each dashed line shows the fitting curve.

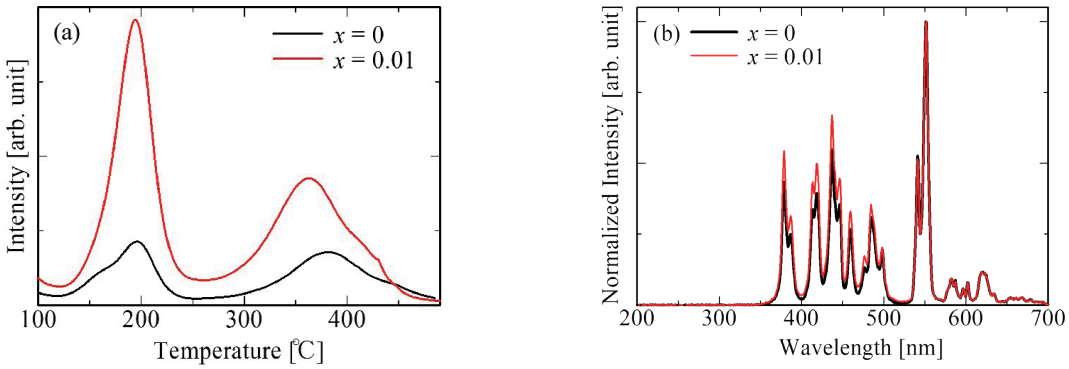

Fig. 4. (Color online) (a) TSL glow curves and (b) TSL spectra heated at 190 ℃ of the $x = 0$ and 0.01 samples. The intensities of the TSL glow curves were corrected for the weight of each sample, and those of TSL spectra were normalized by the intensity at 550 nm.

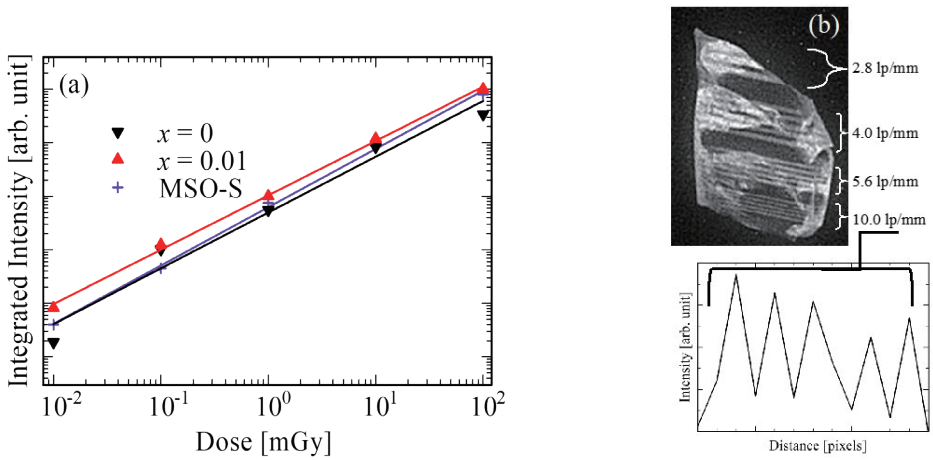

Fig. 5. (Color online) (a) TSL dose response functions of the $x = 0$ and 0.01 samples and MSO-S element. The TSL intensities of the TSL glow curves were corrected for the weight of each sample. (b) X-ray image of the $x = 0.01$ sample and the intensity profile perpendicular to the line pattern (10.0 lp/mm).

of 0.01–100 mGy. The integrated intensity of the $x = 0.01$ sample was higher than that of both the MSO-S element and the $x = 0$ sample.

Figure 5(b) shows an X-ray image of the $x = 0.01$ sample and the intensity profile perpendicular to the line pattern (10.0 lp/mm). Each X-ray test chart had line widths of 2.8, 4.0, 5.6, and 10.0 lp/mm (178.6, 125.0, 89.3, and 50.0 μm, respectively). Except for in the parts with cracks, the emission lines were clearly observed. In the intensity profile in the part with 10 lp/mm, five sharp peaks were observed, and we concluded that the $x = 0.01$ sample had a spatial resolution of 50.0 μm. This spatial resolution is comparable to those of commercially available imaging plates.[40]

4. Conclusions

Both the $x = 0$ and 0.01 samples showed PL emissions due to the 4f–4f transitions of Tb^{3+} ions, and the $x = 0.01$ sample showed PL emissions due to the 5d–4f transitions of Ce^{3+} ions. Regarding the TSL properties, the $x = 0.01$ sample exhibited glow peaks at 190 and 380 °C, and the luminescence centers were only Tb^{3+} ions. The $x = 0.01$ sample showed a linear relationship between dose and integrated intensity from 0.01 to 100 mGy and higher TSL intensity than the $x = 0$ sample and MSO-S elements. In addition, the $x = 0.01$ sample had a spatial resolution of 50.0 μm. In conclusion, the usefulness of the $x = 0.01$ sample as a personal dosimeter and for dose distribution measurement was demonstrated.

Acknowledgments

This work was supported by Grants-in-Aid for Scientific Research A (22H00309), Scientific Research B (22H02939, 21H03733, and 21H03736), and Exploratory Research (22K18997) from the Japan Society for the Promotion of Science. The Cooperative Research Project of the Research Center for Biomedical Engineering, TEPCO Memorial Foundation, Nakatani Foundation, and KRF Foundation are also acknowledged.

References

1 C. W. E. van Eijk: Phys. Med. Biol. **47** (2002) R85.
2 S. K. Mehta, S. Sengupta, and I. K. Oommen: Nucl. Instruments Methods Phys. Res. **197** (1982) 459.
3 P. Covens, D. Berus, N. Buls, P. Clerinx, and F. Vanhavere: Radiat. Prot. Dosim. **124** (2007) 250.
4 T. Yanagida, G. Okada, and N. Kawaguchi: J. Lumin. **207** (2019) 14.
5 J. Seco, B. Clasie, and M. Partridge: Phys. Med. Biol. **59** (2014) R303.
6 T. Kato, D. Shiratori, M. Iwao, H. Takase, D. Nakauchi, N. Kawaguchi, and T. Yanagida: Sens. Mater. **33** (2021) 2163.
7 K. Ichiba, Y. Takebuchi, H. Kimura, D. Shiratori, T. Kato, D. Nakauchi, N. Kawaguchi, and T. Yanagida: Sens. Mater. **34** (2022) 677.
8 R. Oh, S. Yanagisawa, H. Tanaka, T. Takata, G. Wakabayashi, M. Tanaka, N. Sugioka, Y. Koba, and K. Shinsho: Sens. Mater. **33** (2021) 2129.
9 T. Kato, D. Nakauchi, N. Kawaguchi, and T. Yanagida: Sens. Mater. **34** (2022) 653.
10 H. Nanto, G. Okada, K. Hirasawa, Y. Koguchi, W. Shinozaki, S. Ueno, Y. Yanagida, F. D'Errico, and T. Yamamoto: Sens. Mater. **34** (2022) 757.
11 H. Masai, Y. Yanagida, H. Kawamoto, Y. Koguchi, M. Koshimizu, and M. Yamawaki: Sens. Mater. **34** (2022) 699.

12 Y. Takebuchi, T. Kato, D. Nakauchi, N. Kawaguchi, and T. Yanagida: Sens. Mater. **34** (2022) 645.
13 K. Ichiba, Y. Takebuchi, H. Kimura, T. Kato, D. Nakauchi, N. Kawaguchi, and T. Yanagida: Jpn. J. Appl. Phys. **61** (2022) 062006.
14 P. Molina, M. Prokic, J. Marcazzó, and M. Santiago: Radiat. Meas. **45** (2010) 78.
15 E. Bortolin, P. Fattibene, C. Furetta, and S. Onori: Appl. Radiat. Isot. **44** (1993) 327.
16 M. Prokić and E. G. Yukihara: Radiat. Meas. **43** (2008) 463.
17 H. Tawara, M. Masukawa, A. Nagamatsu, K. Kitajo, H. Kumagai, and N. Yasuda: Radiat. Meas. **46** (2011) 709.
18 A. J. J. Bos: Radiat. Meas. **41** (2006) S45.
19 E. Öztürk and E. Karacaoglu: Bull. Mater. Sci. **40** (2017) 25.
20 L. Lin, M. Yin, C. Shi, and W. Zhang: J. Alloys Compd. **455** (2008) 327.
21 M. Jia, J. Wen, X. Pan, Z. Xin, F. Pang, L. He, and T. Wang: Opt. Express **29** (2021) 1210.
22 V. Altunal, V. Guckan, A. Ozdemir, A. Ekicibil, F. Karadag, I. Yegingil, Y. Zydhachevskyy, and Z. Yegingil: J. Alloys Compd. **876** (2021) 160105.
23 T. Matsuo, T. Kato, H. Kimura, F. Nakamura, K. Hashimoto, D. Nakauchi, N. Kawaguchi, and T. Yanagida: J. Lumin. **231** (2021) 117803.
24 Y. Takebuchi, H. Fukushima, T. Kato, D. Nakauchi, N. Kawaguchi, and T. Yanagida: Radiat. Phys. Chem. **177** (2020) 109163.
25 T. Yanagida, Y. Fujimoto, N. Kawaguchi, and S. Yanagida: J. Ceram. Soc. Jpn. **121** (2013) 988.
26 Y. Zhao, S. Qiao, Y. Wang, X. Wu, D. Poelman, and P. D. Townsend: J. Lumin. **228** (2020) 117635.
27 C. Zhao, Y.-H. Wu, D.-H. Wang, S.-X. Cao, S.-Y. Chen, L.-L. Peng, and D.-C. Zhu: J. Lumin. **207** (2019) 241.
28 K. Ichiba, Y. Takebuchi, H. Kimura, T. Kato, D. Nakauchi, N. Kawaguchi, and T. Yanagida: J. Mater. Sci.-Mater. Electron. (2022).
29 K. Ichiba, Y. Takebuchi, H. Kimura, T. Kato, D. Nakauchi, N. Kawaguchi, and T. Yanagida: J. Mater. Sci.-Mater. Electron. **32** (2021) 25065.
30 N. Kawaguchi, D. Nakauchi, T. Kato, Y. Futami, and T. Yanagida: Sens. Mater. **34** (2022) 725.
31 T. Yanagida, T. Kato, D. Nakauchi, and N. Kawaguchi: Sens. Mater. **34** (2022) 595.
32 D. Nakauchi, H. Fukushima, T. Kato, N. Kawaguchi, and T. Yanagida: Sens. Mater. **34** (2022) 611.
33 G. Ito, H. Kimura, D. Shiratori, D. Nakauchi, T. Kato, N. Kawaguchi, and T. Yanagida: Sens. Mater. **34** (2022) 685.
34 D. Nakauchi, T. Kato, N. Kawaguchi, and T. Yanagida: Sens. Mater. **33** (2021) 2203.
35 K. Ichiba, Y. Takebuchi, H. Kimura, T. Kato, D. Shiratori, D. Nakauchi, N. Kawaguchi, and T. Yanagida: Radiat. Phys. Chem. **202** (2023) 110515.
36 S. Akça, Z. G. Portakal, T. Dogan, N. Kucuk, A. Canimoglu, M. Topaksu, and N. Can: Nucl. Instrum. Methods Phys. Res., Sect. B **458** (2019) 12.
37 Y. Zhao, Y. Zhou, Y. Jiang, W. Zhou, A. A. Finch, P. D. Townsend, and Y. Wang: J. Mater. Res. **30** (2015) 3443.
38 S. C. Prashantha, B. N. Lakshminarasappa, and B. M. Nagabhushana: J. Alloys Compd. **509** (2011) 10185.
39 S. C. Prashantha, B. N. Lakshminarasappa, and F. Singh: J. Lumin. **132** (2012) 3093.
40 D. Shiratori, Y. Takebuchi, T. Kato, D. Nakauchi, N. Kawaguchi, and T. Yanagida: Sens. Mater. **34** (2022) 745.